ACS Photonics

pubs.acs.org/journal/apchd5

Letter

On-Chip Transferrable Microdisk Lasers

Sun-Wook Park,[†] Min-Woo Kim,[†] Kyong-Tae Park,[†] Ja-Hyun Ku, and You-Shin No*

Cite This: *ACS Photonics* 2020, 7, 3313−3320

Read Online

ACCESS | Metrics & More | Article Recommendations | Supporting Information

ABSTRACT: Si photonics has been receiving substantial attention as an integration platform in photonics and optoelectronic research, owing to the ability to manufacture low-cost, compact integrated circuits. However, realizing efficient and high-quality light sources remains a major challenge. Herein, we report an on-chip transferrable low-threshold single microdisk laser, which is fabricated by the microtransfer printing using a structured polymer. The optically transparent and adhesive microtip enables readily reproducible, damage-free, and precisely aligned targeted transfer of a single microdisk in the growth substrate onto a prefabricated Si-post on a silicon-on-insulator wafer. Spectroscopic measurements revealed that the microdisk laser with a small Si-post exhibits rich lasing actions with an estimated threshold of ∼96.8 μW. A controlled experiment revealed that laser devices with varied Si-post sizes exhibit no significant changes in optical properties until the size of the Si-post becomes comparable with that of the microdisk. These observations agreed with the results of systematic three-dimensional numerical simulations. We believe that our microtransfer printing technique can be used to transfer micro- and nanostructures onto targeted locations and realize complex microscale heterogeneous architectures in a compact integrated circuit.

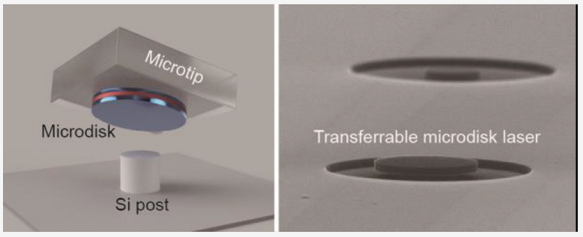

KEYWORDS: *microdisk cavities, microlasers, transfer printing, hybrid integration, electromagnetic simulation, integrated photonic circuits*

Rapid advancements in photonic integration technology require a platform that enables cost-effective, high-density, and seamless integration in a small physical volume while maintaining strong light confinement and low optical loss.[1−4] Si photonics using advanced semiconductor manufacturing processes has made substantial progress, for example, various Si-based photonic applications ranging from tele- and data communications to sensing have been developed, making Si photonics the most promising candidate among others.[5−10] The full potential of Si photonics to realize compact integrated photonic circuits, however, is limited by long-standing challenges related to the efficient integration of high-quality light sources (i.e., lasers). Although some strategies to obtain efficient light emission from Si or compatible materials have been devised, they are only partly successful. This has resulted in insufficient light generation for practical applications or limited operation times.[11,12] Heterogeneous integration using the metallic bonding method has demonstrated successful transfer of prefabricated III−V lasers to Si substrates; however, precise alignment, which is essential for devices with high sensitivity and tunability, remains challenging.[13,14] Furthermore, direct bonding of the III−V epitaxial structure to Si waveguides formed on silicon-on-insulator (SOI) has demonstrated the integration of multiple devices in a single bonding step.[15,16] This approach, however, requires the bonding of large areas of material[15,16] and the planarized nanoscale oxide layer between the III−V material and SOI waveguide,[16] resulting in a wafer-size mismatch and considerably inefficient use of III−V material.

With an increasing demand for faster, more efficient, and compact Si photonics, a more elaborate strategy is required for III−V/Si integration. This strategy should particularly enable individually addressable precise alignment on a target site without sacrificing efficient material use and hampering other devices in a circuit on the same chip. Moreover, the desired III−V lasers must not only be sufficiently small to aid integration density and compactness, but also be capable of generating sufficient amount of light to operate the circuit; for example, low-threshold microlasers with device footprints of approximately few tens of μm^3 can be a promising candidate. In this regard, the recently developed transfer-printing method, which exhibits the ability to selectively pick-up and place small III−V materials on Si, potentially meets the requirements.[17−25] Several pioneering works have already demonstrated the potential. For example, the nanoscale light sources were successfully transferred onto receiving substrates via the membrane-release technique, suspended frame transfer, and the structured polymer-based microtransfer.[20−22] Moreover, the recent demonstration of the targeted transfer of fully fabricated single device enabling the realization of highly functional optical devices has strongly motivated researchers to

Received: August 25, 2020
Published: December 3, 2020

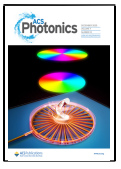

extensively explore the technique to develop the on-chip transferrable microscale light sources in Si photonics.[23−25]

Therefore, in this Letter, we report on-chip transferrable low-threshold microdisk lasers by utilizing the microtransfer printing using a structured polymer. We designed and fabricated an optically transparent, adhesive polymer microtip and utilized it to successfully transfer single microdisks on a growth substrate to predefined Si-posts on a SOI wafer. Spectroscopic measurements were performed to quantitatively investigate the characteristics of the transferred microdisk lasers. A controlled experiment revealed Si-post dependent optical properties, which were verified via numerical simulations.

Figure 1a schematically illustrates our on-chip transferrable microdisk laser device consisting of a high-index semiconductor microdisk cavity (blue disk), including an optical gain medium (red line) and a small circular Si-post that supports the entire cavity structure. The prefabricated single microdisk cavity is separated from its growth substrate by an optically transparent and adhesive microscale cubic polymer tip, which protrudes into the air. This polymer microtip-assisted microtransfer printing allows for real-time bright-field microscopic imaging while approaching, aligning, and contacting microscale structures and materials. Consequently, it enables a straightforward, damage-free, and directly targeted transfer of the microscale structures and materials within and between wafers with high precision and alignment accuracy. The separated microdisk cavity is then brought to the device substrate, center-to-center aligned, and contact-transferred to the target Si-post. The Si-post physically supports the cavity by making contact only with the central area of the microdisk, resulting in an air−semiconductor interface on the cavity periphery, where the high-quality (high-Q) whispering gallery modes (WGMs) are located. As a result, the transferred microdisk cavity can strongly confine the resonant WGMs without disturbing the fields of optical modes and causing any optical loss by the post structure. Figure 1b shows a representative scanning electron microscope (SEM) image of a successfully fabricated on-chip transferrable microdisk laser. The microdisk cavity includes six InGaAsP quantum wells with a central emission wavelength of ∼1550 nm. The cavity structure was robustly supported and center-balanced by a Si-post located underneath. Furthermore, the air-suspended outer region of the microdisk cavity was clearly observed, which can be beneficial to the successful excitation of the high-Q and low-loss resonant WGMs and subsequent low-threshold lasing operation.

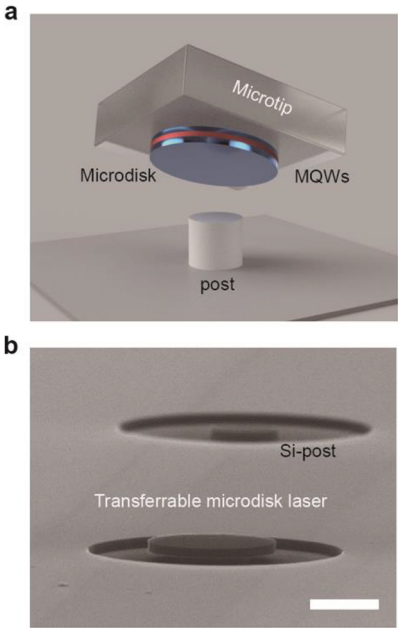

Figure 1. On-chip transferrable microdisk laser. (a) Schematic of the microtransfer printing using a structured polymer. A single microdisk cavity (blue color), which includes multiquantum wells (MQWs, red color), is selectively picked up by a transparent polymer microtip and transferred onto a prefabricated microscale post in a receiving device substrate. (b) Tilted-view SEM image of an InGaAsP microdisk laser device transferred onto a Si-post. The diameter and thickness of the InGaAsP microdisk are 4.2 μm and 260 nm, respectively. The circular Si-post with a diameter of 2.4 μm and thickness of 260 nm is fabricated on a silicon-on-insulator (SOI) wafer. Scale bar: 2 μm.

Our on-chip transferrable microdisk structure was fabricated using the following processes (Figure 2a−d; Figures S1 and S2 of the Supporting Information). First, we used an InGaAsP MQWs wafer and fabricated an array of microdisks with a diameter of ∼4.2 μm via electron-beam lithography and dry etching (Figure 2a, left). After cleaning the residual resist, the sample was dipped in diluted hydrochloric acid solution to partially remove the InP sacrificial layer underneath the microdisk and form a central InP-post with a submicron-size of ∼600 nm (Figure 2a, right). Next, arrays of Si-posts with various diameters were fabricated via another round of electron-beam lithography and dry etching on a SOI wafer (Figure 2b). The dry-etched concentric ring that surrounded the central Si-post serves as a useful geometrical reference with circular symmetry, when aligning a microdisk center-to-center with the Si-post. Furthermore, we prepared an optically transparent and adhesive polydimethylsiloxane (PDMS) microtip using an Si master-mold with a relief pattern of microcubic structures with the dimensions of 20 μm × 20 μm × 20 μm. We then applied either ultraviolet (UV) radiation or oxygen plasma treatment to the fabricated PDMS microtip to achieve a proper level of viscosity for microtransfer printing.[26] The fabrication procedure and PDMS modification are detailed in Supporting Information (Methods, Figure S2). To complete the fabrication of our device, we performed microtransfer printing using a PDMS microtip (Figure S3 of the Supporting Information). Figure 2c displays the schematics (left, (i)−(v)) and the optical microscope images (right, (i)−(ii) and (iv)−(v)) of the key steps of the transfer process. First, the microtip was moved toward a single microdisk, while adjusting the XYZ microtranslation stage to locate the tip and select only the target object ((i), Figure 2c). After establishing contact with the microdisk, we slid the tip in either the x- or y-direction slightly to break the submicron InP-post, and pulled it up to separate the microdisk from its growth substrate ((ii), Figure 2c). Subsequently, the microdisk attached to the bottom of the PDMS tip was subjected to additional wet etching in diluted hydrochloric acid solution to completely remove the broken residues of InP-post ((iii), Figure 2c). Then, we brought the microtip with the microdisk near the location where the target Si-post was fabricated, and aligned the microdisk with the Si-post until their centers were aligned vertically. Here, the Si-posts were additionally surface-treated to increase the interface bonding (Methods in the Supporting Information). As mentioned earlier, the dry-etched ring pattern surrounding the Si-post was useful in enhancing the alignment

https://dx.doi.org/10.1021/acsphotonics.0c01330
ACS Photonics 2020, 7, 3313−3320

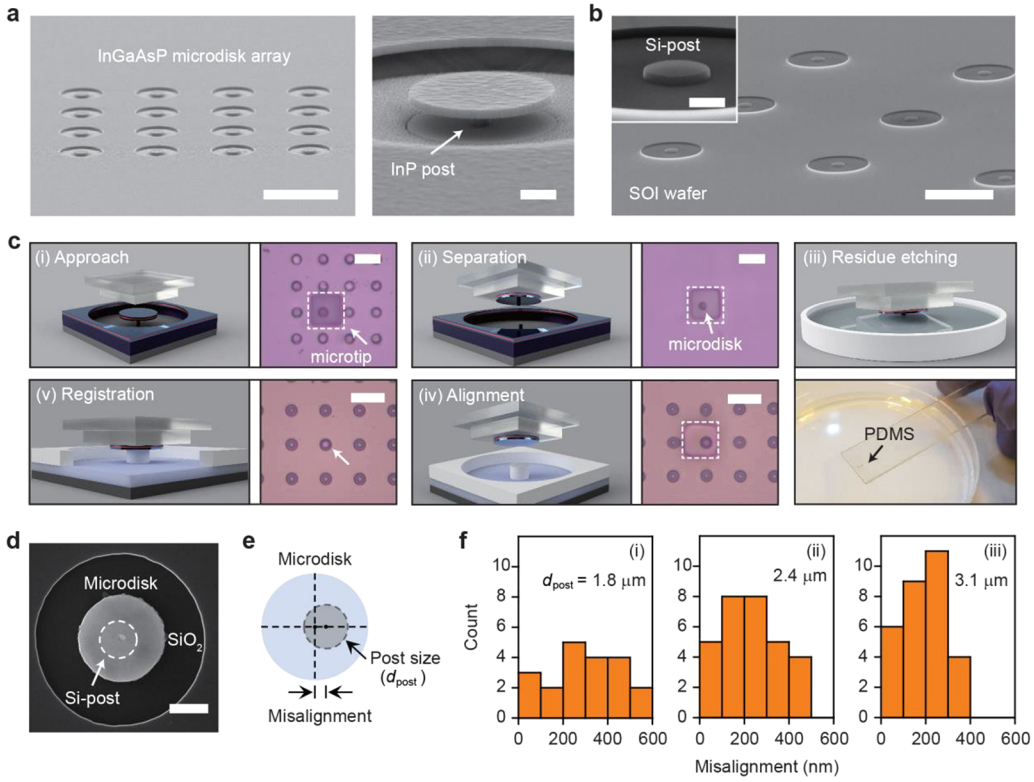

Figure 2. Fabrication of on-chip transferrable microdisk cavity. (a) Tilted-view SEM images of InGaAsP microdisk cavity array (left) and single microdisk cavity (right). Diameter of the microdisk: 4.2 μm. The central InP post with a submicron size of ~600 nm was achieved through selective and anisotropic chemical etching (right). Scale bar: 30 μm (left) and 1 μm (right), respectively. (b) Tilted-view SEM image of an array of Si-posts. Scale bar: 10 μm. Inset: high-magnification SEM image of a single Si-post with a diameter of ~1.8 μm and thickness of 260 nm. Scale bar: 1 μm. (c) Schematics (left, (i)−(v)) and optical microscope images (right, (i)−(ii), (iv)−(v)) of the PDMS microtip-assisted transfer process. (i) Microtip approach to a target microdisk in the growth substrate for adhesive contact (left). The white dotted box represents a microtip (right). (ii) Mechanical separation of the target microdisk by breaking the submicron InP-post (left). A separated single microdisk attached to the microtip (right). (iii) Selective wet etching of the residual InP-post underneath the microdisk (top). Photograph showing the wet etching (bottom) (iv) Center-to-center alignment of the microdisk with a target Si-post. (v) Registration of the microdisk on the Si-post (left). Single microdisk cavity (white arrow) on the Si-post after completion of the transfer (right). All scale bars in the optical microscope images are 20 μm. (d) Top-view SEM image of the transferred microdisk. The white dotted circle indicates the Si-post underneath the microdisk. Scale bar: 2 μm. (e) Schematic showing the misalignment between the microdisk and Si-post with size of d_{post}. (f) Measured misalignment distribution obtained from the transferred microdisks on various Si-posts with different sizes: (i) total of 20 microdisks on Si-posts with a d_{post} of 1.8 μm, (ii) total of 30 microdisks on Si-posts with a d_{post} of 2.4 μm, and (iii) total of 30 microdisks on Si-posts with a d_{post} of 3.1 μm.

precision. Finally, we registered the microdisk on the target site by establishing direct contact with the Si-post and maintaining this position for a few minutes until they were firmly attached to each other. To complete the process, we slowly peeled back the PDMS microtip by simultaneously pulling it up in the vertical direction and translating it in the lateral direction. Figure 2d shows the successfully transferred InGaAsP microdisk cavity on the Si-post (white dotted circle). The cross-sectional SEM images clearly exhibit the high quality of bonding at the interface (Figure S4, Supporting Information). The slightly off-centered alignment is primarily attributed to the resolution limit of our microscope system comprising a 20× long-working-distance objective lens with a numerical aperture of 0.42. The resolution of this microscope system and the corresponding precision of our transfer method can be increased by using an objective lens with a higher magnification and numerical aperture. Because the described fabrication steps, including the microtransfer printing using PDMS microtip, are simple and straightforward, the device yield is high and the final structures are readily reproducible. To directly demonstrate the high yield and reproducibility, and the inevitable misalignment, we fabricated a large number of microdisks and successfully transferred them on various Si-posts with different post size of d_{post} (Figure S5 of the Supporting Information). In addition, we investigated the misalignment distributions for d_{post} of 1.8, 2.4, and 3.1 μm by measuring the distance between the centers of microdisk and Si-post (Figure 2e). The results are shown in Figure 2f. Although the graphs exhibited slightly different distributions, most microdisks on Si-posts were misaligned within 400 nm, which can be explained by the above-mentioned limitations. Furthermore, we examined the mechanical stability of the transferred microdisks on the Si-posts by performing a simple experiment. We again transferred a number of microdisks on the Si-posts with different d_{post} values. We then spin-coated the samples with typical electron-beam resist and compared the number of microdisks before and after the process (Figure S7 of the Supporting Information). The result showed that no missing microdisk was found after the spin-coating. This directly exhibits the mechanical robustness of our devices and also indicates that additional fabrication steps including lithography can be further proceeded.

Then, we performed numerical simulations using the three-dimensional (3D) finite-difference time-domain (FDTD)

https://dx.doi.org/10.1021/acsphotonics.0c01330
ACS Photonics 2020, 7, 3313−3320

method to qualitatively investigate the optical properties of the resonant modes supported by the transferred microdisk cavity (Figure S6(a) of the Supporting Information). We calculated the resonant mode profiles, Q-factor, and mode volume of the transferred microdisk on the Si-post. The diameter and thickness of the microdisk (Si-post) were set to 4.5 μm (2.0 μm) and 260 nm (260 nm), respectively, similar to those of the fabricated structure. The top- and side-views of the calculated electric field intensity profiles show the excited WGM in the cavity, revealing strong confinement of the fields at the boundary of the microdisk. The Q-factor and mode volume (V_m) were calculated as ~2.5 × 10^6 and ~1.6 μm^3, respectively, which are comparable to those of the free-standing microdisk cavity without Si-post; this indicates that the central Si-post with a small diameter does not significantly influence the optical properties of the excited WGMs. In addition, we investigated the effect of misalignment on the Q-factor and resonant wavelength of the WGM by introducing the off-center distance d_{OFF} between the centers of microdisk and Si-post (Figure S6 of the Supporting Information). The result showed a significant decrease in Q-factor at d_{OFF} > 400 nm and further decrease at d_{OFF} > 800 nm. For the resonant wavelength, it remained almost unchanged until d_{OFF} = 600 nm, which revealed that the WGM experienced no significant index variation. However, the wavelength exhibited an abrupt red-shift at d_{OFF} > 800 nm, showing the noticeable transmission of fields through the microdisk and Si-post (Figure S6(c) of the Supporting Information). Considering the misalignment distributions in Figure 2f, the simulation result confirms that the transferred microdisks barely sacrifice their intrinsic optical properties.

We carried out photoluminescence (PL) spectroscopy to investigate the optical characteristics of our on-chip transferrable microdisk cavity. The fabricated microdisk cavity in Figure 2d was optically pumped at room temperature by a pulsed laser diode with a wavelength of 976 nm (100 ns pulses of ~10% duty cycle). A 50× microscope objective lens was used to focus the pump beam to a spot of size ~3.9 μm and to collect the light from the device. The PL was then either fed into the spectrometer or imaged onto an infrared (IR) camera (Figure S8 of the Supporting Information). As the incident pump power increased, a sharp and pronounced peak was detected, along with a rapid increase in intensity. At the further increased incident powers, we observed rich lasing actions from the microdisk cavity. Figure 3a shows the normalized above-threshold PL spectrum measured from the cavity. A pronounced lasing peak at the wavelength of 1542.2 nm was observed. In addition, we captured a lasing mode image using the IR camera, which reveals strong light emission at the boundary of the microdisk cavity (inset of Figure 3a). To clearly characterize the transition to the lasing mode, we systematically measured both the collected output intensity and the spectral line width of the mode as a function of the incident peak pump power (Figure 3b). In the plot, the peak intensity in each spectrum was normalized with respect to the maximum value. A superlinear increase in output intensity was clearly observed at an estimated lasing threshold of ~143.4 μW. Note that the estimated threshold is comparable to those of previously reported microdisk lasers with a similar size and even a smaller supporting InP-post mounted on the growth substrate.[27,28] This result experimentally corroborates the numerical result obtained above, that is, the Si-post underneath the transferred microdisk cavity does not significantly influence

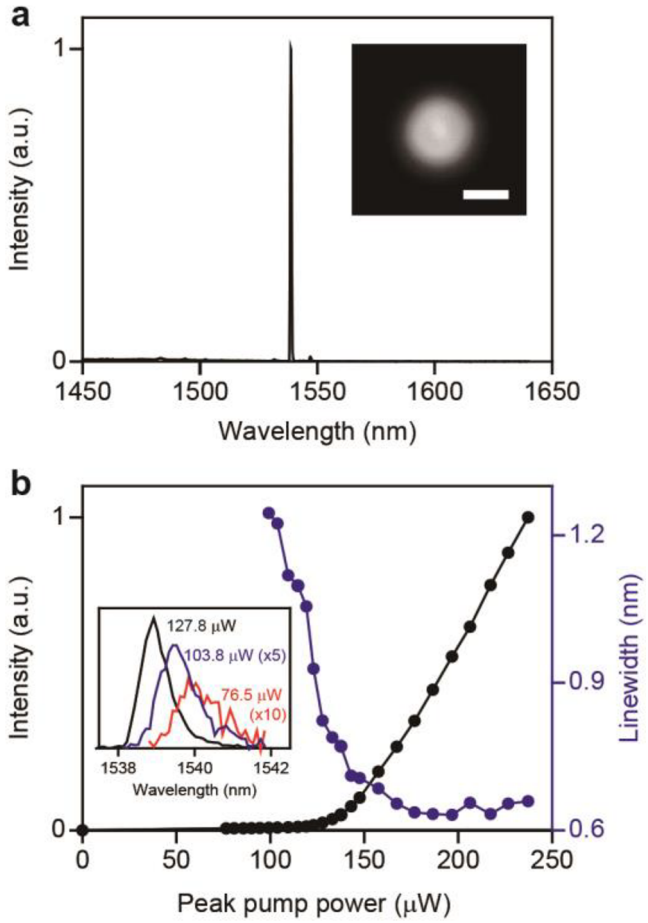

Figure 3. Transferrable microdisk laser. (a) Above-threshold lasing spectrum measured at a peak pump power of 162.6 μW. Pulsed laser diode, with a wavelength of 976 nm, was used to pump the laser device. Pulse width and repetition rate were 100 ns and 1 MHz, respectively. Strong lasing action was observed at a wavelength of 1542.2 nm. Inset shows the lasing mode image captured by an IR camera at a peak pump power of 176.8 μW. Scale bar: 5 μm. (b) Measured lasing intensity and spectral line width of the lasing mode as a function of the incident peak pump power. The threshold peak power is ~143.4 μW. Inset shows below- and near-threshold PL spectra measured at different peak pump powers of 76.5 (red), 103.8 (blue), and 127.8 μW (black), respectively.

the optical properties of the cavity. We also note that the estimated threshold can be lower at the decreased duty ratios <10% since the pump-induced heating on a device can be sufficiently suppressed (Figure S9 of the Supporting Information). For example, we observed a reduced threshold of ~96.8 μW from the device with d_{post} of ~1.8 μm at duty ratio of 5%. Further, the control experiment in Figure S9 exhibits the laser device on the Si-post showed the lower lasing thresholds at various pumping conditions compared with those obtained from the device on the InP-post with similar size. This can be partly explained with both the difference of heat flow via the bonded interface and the epitaxial hetero-interface and the difference of the thermal conduction between InP and Si.[29,30] A more detailed numerical study of heat transfer is presented in Figure S10 (Supporting Information), which revealed the stationary temperature distributions of the microdisk devices on various Si-posts and planar substrates. As the incident pump power was increased from below the threshold to above the threshold, the measured spectral line

https://dx.doi.org/10.1021/acsphotonics.0c01330
ACS Photonics 2020, 7, 3313−3320

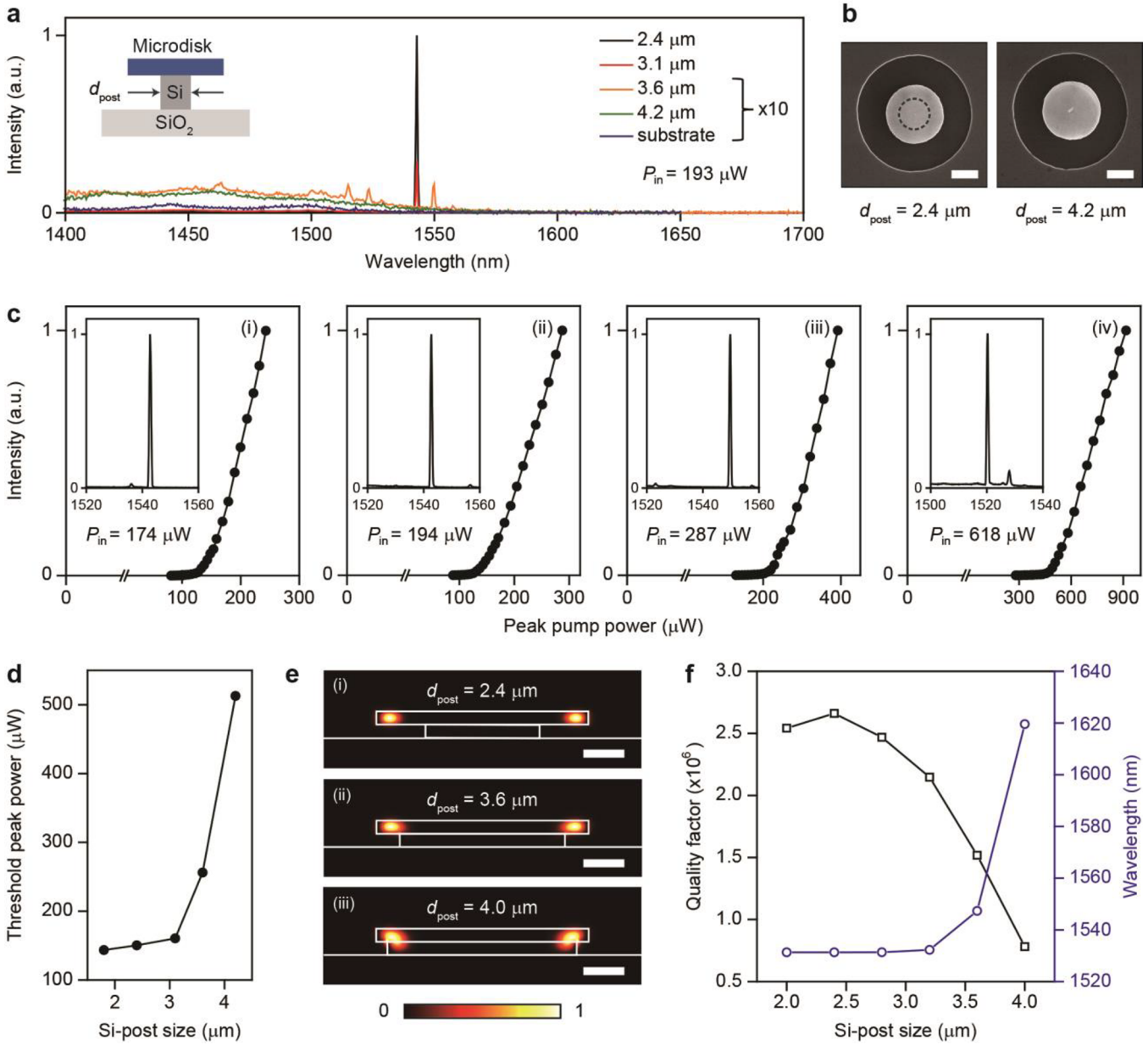

Figure 4. Lasing behaviors with various sizes of Si-post. (a) Measured PL spectra from the transferred microdisks on five different sizes of Si-posts (d_{post}, inset). The measured d_{post} values are 2.4 (black), 3.1 (red), 3.6 (yellow), and 4.2 μm (olive). A spectrum of the microdisk on the Si-substrate (d_{post} = infinite) is also coplotted (blue). The diameters of all microdisks used in the experiment were fixed at 4.2 μm. The intensities were normalized with the maximum intensity value in the spectrum for d_{post} = 2.4 μm for comparison, and the intensities for d_{post} = 3.6 and 4.2 μm and infinity were increased 10-fold for clarity. The incident peak pump power in all measurements was set to 193 μW. (b) Top-view SEM images of the transferred microdisks on two different Si-posts with d_{post} values of 2.4 (left) and 4.2 μm (right). In the left panel, the dotted black circle indicates the Si-post underneath. In the right panel, the tightly aligned microdisk and Si-post have the same diameter. Scale bar: 2 μm. (c) Measured output intensities from the devices in (a) as a function of the incident peak pump power: the characteristic curves of (i)−(iv) are for the laser devices with d_{post} values of 2.4, 3.1, 3.6, and 4.2 μm. The insets are the above-threshold lasing spectra of the individual devices. The incident pump powers were 174, 194, 287, and 618 μW and the corresponding lasing wavelengths are 1542.8, 1542.7, 1549.8, and 1520.3 nm, respectively. (d) Plot of the lasing thresholds from (i)−(iv) in (c) as a function of Si-post size. In the plot, the threshold of the laser device with a d_{post} value of 1.8 μm in Figure 3 is included. (e) Side views of the calculated electric field intensity profiles of the WGMs in the microdisk cavities with various d_{post} values of (i) 2.4, (ii) 3.6, and (iii) 4.0 μm. Diameter of the microdisk cavity was set to 4.5 μm. (f) Calculated Q-factors and resonant wavelengths plotted as a function of Si-post size.

widths of the lasing mode decreased drastically near the threshold and became resolution-limited of the spectrometer (~0.65 nm). The below- and near-threshold spectra shown in the inset of Figure 3b reveal this abrupt change in the line width. From the line width of the peak at a transparency peak pump power of ~127.8 μW, the experimental Q-factor of the cavity ($Q = \lambda/\Delta\lambda$) was estimated to be >1800, which is comparable to that reported in previous studies.[31,32]

Obtaining intact optical properties from our laser device without causing any undesired optical losses and spectral variations primarily depends on the size of the Si-post if the post and microdisk are center-aligned. Consequently, it is

https://dx.doi.org/10.1021/acsphotonics.0c01330
ACS Photonics 2020, 7, 3313−3320

important to estimate the maximum possible size of the Si-post that can guarantee the original optical properties of the microdisk cavity and, correspondingly, the laser device. To experimentally address this problem, we examined the viability of achieving lasing action from various laser devices with microdisk cavities of the same diameter (i.e., 4.2 μm; similar to that in Figure 3), but with Si-posts of different sizes. Figure 4a shows the measured spectra from the transferred microdisk cavities with four different Si-post sizes (d_{post}, inset) as follows: 2.4 (black), 3.1 (red), 3.6 (yellow), and 4.2 μm (olive). The spectrum obtained from the microdisk on an Si substrate was also co-plotted for regarding it as an infinite size of Si-post. All spectra were measured under the same incident peak pump power of 193 μW. In the plot, the intensities of all spectra were normalized with the maximum intensity value in the lasing spectrum with a d_{post} of 2.4 μm, and the intensities from d_{post} of 3.6 and 4.2 μm and infinity were then increased 10-fold for clarity. All microdisks were center-transferred to the Si-posts with minimum misalignment. Representative SEM images of the devices with d_{post} values of 2.4 and 4.2 μm are shown in Figure 4b. In Figure 4a, strong lasing actions from the devices with d_{post} of 2.4 and 3.1 μm are clearly observed, whereas no lasing operation is observed from those with d_{post} of 3.6 and 4.2 μm and infinity. These results reveal several interesting features. First, the measured spectral positions of the lasing modes from the two devices (1542.8 nm (black, 2.4 μm), and 1542.7 nm (red, 3.1 μm)) are almost the same, although the lasing peak intensities are different. Further, the measured spectrum in Figure 3a shows a lasing peak at 1542.2 nm, which directly indicates that the same resonant WGMs were excited in the individual cavities and developed to be the lasing modes. Correspondingly, this reveals that the resonant modes that are located at the boundary of the cavity barely experience a difference in effective index between the three devices, but have slightly different lasing thresholds. Second, the device with a d_{post} value of 3.6 μm shows a nonlasing but dominant peak at 1549.8 nm. Notably, this spectral red-shift of ~7 nm with below-threshold spectral behavior unambiguously signifies that the optical properties of the microdisk cavity are affected by the enlarged Si-post. Third, no noticeable peaks from the devices with a d_{post} value of 4.2 μm and infinity are observed under the given incident peak pump power. This suggests that the Si-post with a size >4 μm, which is almost comparable to the size of the microdisk cavity, severely alters the original optical properties of the cavity and serves as a significant optical loss channel. To experimentally verify our analysis of Figure 4a, we measured the above-threshold lasing spectra and subsequently measured the output intensities of each device as a function of the incident peak pump power to obtain the characteristic curves of the laser devices. Figure 4c shows the results for the four devices with finite sizes of Si-posts. All devices exhibited a superlinear behavior, revealing the clear transition to the lasing modes as shown in the insets. As expected, the devices with d_{post} values of 2.4 and 3.1 μm showed slightly different lasing thresholds of ~150.3 ((i), Figure 4c) and ~160.5 μW ((ii), Figure 4c), respectively. In addition, we observed a lasing operation from the device with a d_{post} value of 3.6 μm at a wavelength of 1549.8 nm (inset of (iii), Figure 4c), whose estimated threshold was ~256.1 μW ((iii), Figure 4c). Here, the small increase in threshold, despite the improved heat conduction through the enlarged Si-post, can be partly explained by the increased transmission of the pump beam and emitted light through the post, resulting in a decreased pump efficiency and optical gain in the cavity.

Furthermore, we observed successful lasing actions from the device with a d_{post} value of 4.2 μm at higher incident pump powers, >500 μW (inset of (iv), Figure 4c), which explains the featureless PL spectrum in Figure 4a. Notably, a lasing peak was measured at a wavelength of 1520.3 nm, which is significantly blue-shifted compared with that of all the other devices. We attribute this spectral shift primarily to the excitation of a new resonant mode supported by the combined structure of the microdisk and Si-post. In addition, no detectable lasing action was observed from the device on an Si substrate at the incident pump power <1000 μW. The lasing thresholds observed in Figure 4c are plotted as a function of the Si-post size in Figure 4d.

To further substantiate our analysis and experimental results, we performed 3D FDTD simulations. Figure 4e shows the side views of the calculated electric field intensity profiles of the resonant WGMs excited in the cavities with d_{post} values of 2.4 ((i)), 3.6 ((ii)), and 4.0 μm ((iii)). The resonant WGM mode of (i) is clearly well-confined within the boundary of the cavity; the resonant wavelength of ~1531.3 nm is identical to that in Figure S6(a). However, a small portion of the field in the resonant mode of (ii) extends toward the edge of the Si-post, resulting in a slight variation in the effective index of the mode and a subsequent shift in resonant wavelength (i.e., $\lambda_{(ii)}$ = ~1532.5 nm). However, the field profile in (iii) is completely different from those of the other modes. In this case, a considerable portion of the field is confined at the interface between the microdisk and the Si-post, which can no longer be identified as the same mode excited in (i) and (ii). In addition, we calculated Q-factors and the resonant wavelengths of the mode as a function of d_{post} (Figure 4f). The results show an increase in wavelength and a decrease in Q-factor, as d_{post} increases. In particular, we again observed that the wavelength shifts noticeably near d_{post} > 3.5 μm and increases rapidly thereafter, which strongly supports our experimental observations. Furthermore, the experimentally observed blue-shift of the lasing mode in the device with a d_{post} value of 4.2 μm was successfully explained with the excitation of different WGM with a different azimuthal order (Figure S11 of the Supporting Information).

In conclusion, we used the optically transparent and adhesive PDMS microtip-assisted transfer method to demonstrate on-chip target-transfer of a single microdisk cavity from its growth substrate to a microscale Si-post in a receiving device substrate. This damage-free transfer method allows for simple, straightforward, and precise alignment; furthermore, it enables successful fabrication of transferrable microdisk lasers in an easily reproducible manner. In spectroscopic measurements, we observed low-threshold lasing actions from the devices in which the size of the Si-post was smaller compared with that of the microdisk cavity. On the contrary, we observed an increased threshold and spectral shift from the devices with Si-posts larger than the microdisk cavity. These observations corresponded well to the results of 3D FDTD simulations. We believe that the demonstrated microtransfer printing using a structured polymer can be exploited to realize more complex, on-chip, 3D microstructures for functional devices in ultrasmall photonic integrated circuits.

https://dx.doi.org/10.1021/acsphotonics.0c01330
ACS Photonics 2020, 7, 3313−3320

■ ASSOCIATED CONTENT

Supporting Information

The Supporting Information is available free of charge at https://pubs.acs.org/doi/10.1021/acsphotonics.0c01330.

Detailed description of experimental methods and additional figures (PDF)

■ AUTHOR INFORMATION

Corresponding Author

You-Shin No − *Department of Physics, Konkuk University, Seoul 05029, Republic of Korea;* orcid.org/0000-0001-8947-4189; Phone: +82-2-450 3419; Email: ysno@konkuk.ac.kr; Fax: +82-2-3436-5382

Authors

Sun-Wook Park − *Department of Physics, Konkuk University, Seoul 05029, Republic of Korea*

Min-Woo Kim − *Department of Physics, Konkuk University, Seoul 05029, Republic of Korea*

Kyong-Tae Park − *Department of Physics, Konkuk University, Seoul 05029, Republic of Korea*

Ja-Hyun Ku − *Department of Physics, Konkuk University, Seoul 05029, Republic of Korea*

Complete contact information is available at: https://pubs.acs.org/10.1021/acsphotonics.0c01330

Author Contributions

†These authors have contributed equally to this work.

Notes

The authors declare no competing financial interest.

■ ACKNOWLEDGMENTS

Y.-S.N. acknowledges the support of this work by Konkuk University, 2017.

■ REFERENCES

(1) Liu, A.; Jones, R.; Liao, L.; Samara-Rubio, D.; Rubin, D.; Cohen, O.; Nicolaescu, R.; Paniccia, M. A high-speed silicon optical modulator based on a metal−oxide-semiconductor capacitor. *Nature* **2004**, *427*, 615−618.

(2) Xu, Q.; Schmidt, B.; Pradhan, S.; Lipson, M. Micrometre-scale silicon electro-optic modulator. *Nature* **2005**, *435*, 325−327.

(3) Assefa, S.; Xia, F.; Vlasov, Y. A. Reinventing germanium avalanche photodetector for nanophotonic on-chip optical interconnects. *Nature* **2010**, *464*, 80−84.

(4) Michel, J.; Liu, J.; Kimerling, L. C. High-performance Ge-on-Si photodetectors. *Nat. Photonics* **2010**, *4*, 527−534.

(5) Soref, R. The Past, Present, and Future of Silicon Photonics. *IEEE J. Sel. Top. Quantum Electron.* **2006**, *12*, 1678−1687.

(6) Wang, Z.; Abbasi, A.; Dave, U.; De Groote, A.; Kumari, S.; Kunert, B.; Merckling, C.; Pantouvaki, M.; Shi, Y.; Tian, B.; van Gasse, K.; Verbist, J.; Wang, R.; Xie, W.; Zhang, J.; Zhu, Y.; Bauwelinck, J.; Yin, X.; Hens, Z.; van Campenhout, J.; Kuyken, B.; Baets, R.; Morthier, G.; van Thourhout, D.; Roelkens, G. Novel Light Source Integration Approaches for Silicon Photonics. *Laser Photonics Rev.* **2017**, *11*, 1700063.

(7) Liang, D.; Bowers, J. E. Recent progress in lasers on silicon. *Nat. Photonics* **2010**, *4*, 511−517.

(8) Fang, A. W.; Park, H.; Kuo, Y.-H.; Jones, R.; Cohen, O.; Liang, D.; Raday, O.; Sysak, M. N.; Paniccia, M. J.; Bowers, J. E. Hybrid silicon evanescent devices. *Mater. Today* **2007**, *10*, 28−35.

(9) Roelkens, G.; Van Campenhout, J.; Brouckaert, J.; Van Thourhout, D.; Baets, R.; Romeo, P. R.; Regreny, P.; Kazmierczak, A.; Seassal, C.; Letartre, X.; Hollinger, G.; Fedeli, J.M.; Di Cioccio, L.; Lagahe-Blanchard, C. III-V/Si photonics by die-to-wafer bonding. *Mater. Today* **2007**, *10*, 36−43.

(10) Robinson, J. T.; Chen, L.; Lipson, M. On-chip gas detection in silicon optical microcavities. *Opt. Express* **2008**, *16*, 4296−4301.

(11) Pavesi, L.; Dal Negro, L.; Mazzoleni, C.; Franzò, G.; Priolo, F. Optical gain in silicon nanocrystals. *Nature* **2000**, *408*, 440−444.

(12) Groenert, M. E.; Leitz, C. W.; Pitera, A. J.; Yang, V.; Lee, H.; Ram, R. J.; Fitzgerald, E. A. Monolithic integration of room-temperature cw GaAs/AlGaAs lasers on Si substrates via relaxed graded GeSi buffer layers. *J. Appl. Phys.* **2003**, *93*, 362−367.

(13) Palit, S.; Tsvid, G.; Kirch, J.; Huang, J. Y.-T.; Tyler, T.; Cho, S.-Y.; Jokerst, N.; Mawst, L.; Kuech, T. Top-Bottom Stripe Thin Film InGaAs/GaAsP Laser integrated on Silicon. *Proc. Dev. Res. Conf.* **2008**, 137−138.

(14) Rumpler, J. J.; Fonstad, C. G. Continuous-Wave Electrically Pumped 1.55-μm Edge-Emitting Platelet Ridge Laser Diodes on Silicon. *IEEE Photonics Technol. Lett.* **2009**, *21*, 827−829.

(15) Fang, A. W.; Park, H.; Cohen, O.; Jones, R.; Paniccia, M. J.; Bowers, J. E. Electrically pumped hybrid AlGaInAs-silicon evanescent laser. *Opt. Express* **2006**, *14*, 9203−9210.

(16) van Campenhout, J.; Rojo-Romeo, P.; Regreny, P.; Seassal, C.; van Thourhout, D.; Verstuyft, S.; Di Cioccio, L.; Fedeli, J.-M.; Lagahe, C.; Baets, R. Electrically pumped InP-based microdisk lasers integrated with a nanophotonic silicon-on-insulator waveguide circuit. *Opt. Express* **2007**, *15*, 6744−6749.

(17) Yang, H.; Zhao, D.; Chuwongin, S.; Seo, J.-H.; Yang, W.; Shuai, Y.; Berggren, J.; Hammar, M.; Ma, Z.; Zhou, W. Transfer-printed stacked nanomembrane lasers on silicon. *Nat. Photonics* **2012**, *6*, 615−620.

(18) Justice, J.; Bower, C.; Meitl, M.; Mooney, M. B.; Gubbins, M. A.; Corbett, B. Wafer-scale integration of group III−V lasers on silicon using transfer printing of epitaxial layers. *Nat. Photonics* **2012**, *6*, 610−614.

(19) Ning, H.; Krueger, N. A.; Sheng, X.; Keum, H.; Zhang, C.; Choquette, K. D.; Li, X.; Kim, S.; Rogers, J. A.; Braun, P. V. Transfer-Printing of Tunable Porous Silicon Microcavities with Embedded Emitters. *ACS Photonics* **2014**, *1*, 1144−1150.

(20) Fan, F.; Yu, Y.; Amiri, S. E. H.; Quandt, D.; Bimberg, D.; Ning, C. Z. Fabrication and room temperature operation of semiconductor nano-ring lasers using a general applicable membrane transfer method. *Appl. Phys. Lett.* **2017**, *110*, 171105.

(21) Osada, A.; Ota, Y.; Katsumi, R.; Watanabe, K.; Iwamoto, S.; Arakawa, Y. Transfer-printed quantum-dot nanolasers on a silicon photonic circuit. *Appl. Phys. Express* **2018**, *11*, 072002.

(22) Guilhabert, B.; Hurtado, A.; Jevtics, D.; Gao, Q.; Tan, H. H.; Jagadish, C.; Dawson, D. D. Transfer Printing of Semiconductor Nanowires with Lasing Emission for Controllable Nanophotonic Device Fabrication. *ACS Nano* **2016**, *10*, 3951−3958.

(23) Karnadi, I.; Son, J.; Kim, J.-Y.; Jang, H.; Lee, S.; Kim, K. S.; Min, B.; Lee, Y.-H. A printed nanobeam laser on a SiO_2/Si substrate for low-threshold continuous-wave operation. *Opt. Express* **2014**, *22*, 12115−12121.

(24) Lee, J.; Karnadi, I.; Kim, J. T.; Lee, Y.-H.; Kim, M.-K. Printed Nanolaser on Silicon. *ACS Photonics* **2017**, *4*, 2117−2123.

(25) Guilhabert, B.; Mcphillimy, J.; May, S.; Klitis, C.; Dawson, M. D.; Sorel, M.; Strain, M. J. Hybrid integration of an evanescently coupled AlGaAs microdisk resonator with a silicon waveguide by nanoscale-accuracy transfer printing. *Opt. Lett.* **2018**, *43*, 4883−4886.

(26) Berdichevsky, Y.; Khandurina, J.; Guttman, A.; Lo, Y.-H. UV/ozone modification of poly(dimethylsiloxane) microfluidic channels. *Sens. Actuators, B* **2004**, *97*, 402−408.

(27) Chu, D. Y.; Chin, M. K.; Sauer, N. J.; Xu, Z.; Chang, T. Y.; Ho, S. T. 1.5-μm InGaAs/InAlGaAs Quantum-well Microdisk laser. *IEEE Photonics Technol. Lett.* **1993**, *5*, 1353−1355.

(28) McCall, S. L.; Levi, A. F. J.; Slusher, R. E.; Pearton, S. J.; Logan, R. A. Whispering-gallery mode microdisk lasers. *Appl. Phys. Lett.* **1992**, *60*, 289−291.

(29) Sze, S. M. *Physics of Semiconductor Devices*, 2nd ed.; John Wiley & Sons, 1981.

(30) Tiwari, S. *Compound Semiconductor Device Physics*; Academic Press, 2013.
(31) Bjőrk, G.; Karlsson, A.; Yamamoto, Y. On the linewidth of microcavity lasers. *Appl. Phys. Lett.* **1992**, *60*, 304−306.
(32) Mohideen, U.; Slusher, R. E.; Jahnke, F.; Koch, S. W. Semiconductor Microlaser Linewidths. *Phys. Rev. Lett.* **1994**, *73*, 1785−1788.

https://dx.doi.org/10.1021/acsphotonics.0c01330
ACS Photonics 2020, 7, 3313−3320